ADVANCED ENERGY MATERIALS
www.advenergymat.de

Influence of Carbonate Electrolyte Solvents on Voltage and Capacity Degradation in Li-Rich Cathodes for Li-ion Batteries

*Rui Wang, Bo Weng, Amoghavarsha Mahadevegowda, Israel Temprano, Heng Wang, Ze He, Caterina Ducati, Yinguo Xiao, Clare P. Grey, and Michael F. L. De Volder**

Lithium-rich cobalt-free cathodes, such as $Li_{1.2}Mn_{0.6}Ni_{0.2}O_2$ (LMR), are promising next-generation cathode materials because of their high energy density, cost efficiency, and sustainability. Nevertheless, LMRs suffer from degradation problems such as voltage decay during cycling. Different LMR surface doping and coating strategies are proposed to suppress LMR voltage decay with varying extents of success. Here, the role played by different electrolyte solvents in oxygen loss from the LMR surface is instead investigated. X-ray absorption spectroscopy (XAS), electron energy loss spectroscopy (EELS), synchrotron XRD, and online electrochemical mass spectrometry (OEMS) results show that ethylene carbonate (EC) leads to accelerated oxygen loss from the LMR surface. As a result, cycling LMR cathodes in EC-free electrolytes such as pure EMC, improves the capacity retention and reduces voltage decay. This approach provides a new strategy to increase the cycling stability of LMR cathodes, which is important for the development of more sustainable high-performance batteries.

1. Introduction

Over the course of the last three decades, lithium-ion batteries (LIBs) have emerged as one of the most successful electrochemical energy storage solutions. This technology has enabled the development and commercialization of various portable electronic devices and electric vehicles.[1] However, this commercial success has substantially increased demand for elements used in LIB cathodes such as Li, Ni, and Co, which in turn results in concerns about their future cost as well as the overall sustainability of batteries. Lithium-rich manganese-based cathode materials such as $Li_{1.2}Mn_{0.6}Ni_{0.2}O_2$ (LMR), are particularly interesting to address this issue as they contain no Co and only limited amounts of Ni, while at the same time providing high specific capacities exceeding 250 mAh g^{-1}.[2] These cathode materials have a layered structure similar to more traditional ones, such as $LiNi_xCo_yMn_zO_2$ (NMC), and they can be produced on a large scale using co-precipitation methods. As a result, LMRs have emerged as one of the most promising next-generation cathode materials, holding the potential to achieve energy densities exceeding 400 Wh kg^{-1} at the cell level. However, LMRs face challenges of their own in terms of low first-cycle coulombic efficiency and cycling stability.[3] In particular, discharge voltage decay during cycling poses a significant obstacle to their commercialization.[4]

R. Wang, B. Weng, H. Wang, Z. He, M. F. L. De Volder
Department of Engineering
University of Cambridge
17 Charles Babbage Road, Cambridge CB3 0FS, UK
E-mail: mfld2@cam.ac.uk

R. Wang, A. Mahadevegowda, I. Temprano, H. Wang, C. Ducati, C. P. Grey, M. F. L. De Volder
The Faraday Institution
Quad One
Harwell Science and Innovation Campus
Didcot OX11 0RA, UK

A. Mahadevegowda, C. Ducati
Department of Materials Science & Metallurgy
University of Cambridge
27 Charles Babbage Road, Cambridge CB3 0FS, UK

I. Temprano, C. P. Grey
Department of Chemistry
University of Cambridge
Lensfield Road, Cambridge CB2 1EW, UK

I. Temprano
CICA-Centro Interdisciplinar de Química e Bioloxía and Departamento de Química
Facultade de Ciencias
Universidade da Coruña
A Coruña 15071, Spain

Y. Xiao
School of Advanced Materials
Peking University
Shenzhen Graduate School
Shenzhen 518055, China

The ORCID identification number(s) for the author(s) of this article can be found under https://doi.org/10.1002/aenm.202401097

DOI: 10.1002/aenm.202401097

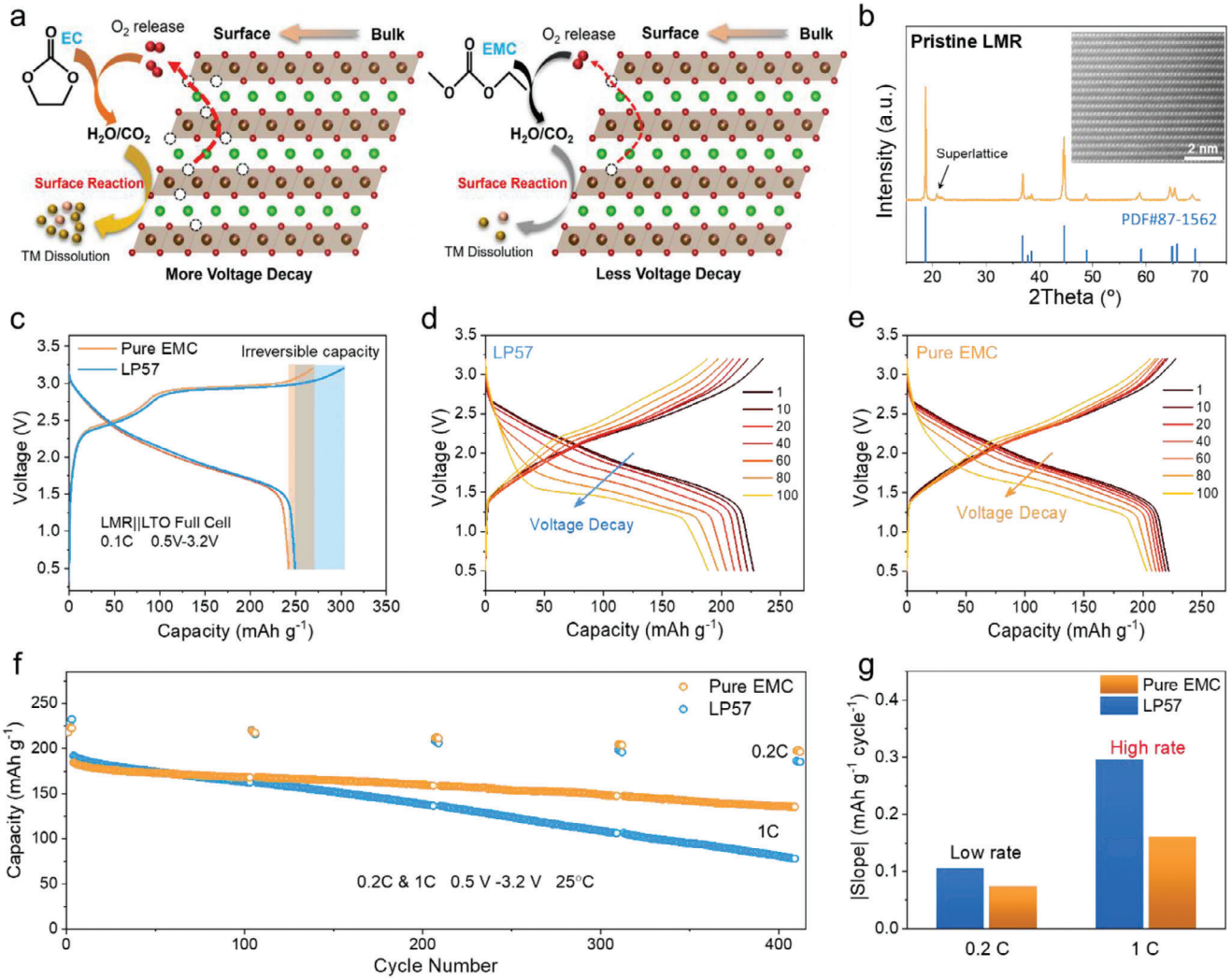

Figure 1. a) Schematic diagram of side reactions between the electrolyte and LMR cathode interface with LP57 and pure EMC electrolyte. b) XRD diffraction pattern for the Pristine LMR cathode, the insert figure is the atomic level TEM image for the Pristine LMR cathode. c) Charge–discharge curves for the first cycle of an LMR||LTO full cell with either LP57 or pure EMC electrolytes at 0.1C in a voltage window of 0.5–3.2 V. d,e) The charge–discharge curves of Li-rich cathode with the LP57 and EMC electrolytes at 0.2 C for different cycles. f) Long term cycling performance at a rate of 1 C over 400 cycles for the LMR||LTO full cell with LP57 and EMC electrolytes with three recovery cycles at 0.2 C carried out after every 100 cycles. g) The absolute value of slope for the full cell's capacity decay versus cycle number with the two types of electrolytes at a low rate of 0.2 C and a high rate of 1 C over 400 cycles.

Recent research results indicate that the fundamental reasons behind these degradation processes are irreversible oxygen release and phase transformation of the LMR cathode surface and subsurface[5] which leads to transition metal dissolution and an avalanche of other complex degradation processes.[6] Here, for the ease of terminology, in the following content of this article, the surface and the subsurface are collectively referred to as surface. Several groups have proposed a range of surface modification strategies to mitigate the side reactions between the cathode and electrolyte interface and improve the cycle stability of the LMR cathode, including surface coating,[7] surface doping,[8] and surface structure optimization.[9]

In this article, we propose an alternative approach, where we first identify that ethylene carbonate (EC) solvent is accelerating oxygen loss from the LMR surface. This is somewhat unexpected because previous studies on NMC have shown that EC only accelerates oxygen loss in Ni-rich (NMC811) cathodes whereas standard NMC formulations with a Ni content similar to our LMR cathodes were not adversely affected by EC.[10] Nevertheless, we confirmed accelerated oxygen loss when using EC solvent in LMRs using X-ray absorption spectroscopy (XAS), electron energy loss spectroscopy (EELS), synchrotron XRD (X-ray diffraction), and online electrochemical mass spectrometry (OEMS). We show that using EC-free electrolytes (here pure EMC) reduces oxygen loss and transition metal dissolution, leading to the overall proposed degradation mechanism depicted in **Figure 1a**, which is in line with previous studies on EC-free electrolytes in NMC811 cells.[10] Further, we observe less capacity degradation and voltage fade in cells using EC-free electrolytes.

This work shows that optimizing the electrolyte composition can play a crucial role in improving the stability of LMR cathodes alongside ongoing work on LMR surface coating and doping.

2. Results

Cobalt-free Li-rich cathodes $Li_{1.2}Mn_{0.6}Ni_{0.2}O_2$ (LMR) are synthesized by a microwave-assisted hydrothermal method followed by high-temperature annealing (see Experimental Section). As-synthesized LMR particles are shown in Figure S1a (Supporting Information) and have diameters ranging between 200 and 500 nm. Figure 1b shows the XRD diffraction pattern of the as synthesized LMR cathode material. Based on a standard α-$NaFeO_2$ structure PDF card (#87-1562),[11] the LMR cathode exhibits an ideal layered structure without any impurity phases detected and the STEM image in the insert figure further shows an ideal layered structure in our LMR cathodes. Also, atomic-level STEM images (Figure S1b, Supporting Information) show that as-prepared LMR cathode surfaces do not show the presence of spinel or rock salt phases. In addition, some weak superstructure peaks in the range of 20–25 degrees are observed, which correspond to the honeycomb Li–Mn ion ordering within the transition metal layer and the honeycomb structure partial ordering along the c-axis.[12] The Raman spectroscopy shown in Figure S2 (Supporting Information) also confirms that the LMR cathode is composed, at least locally, of two environments that resemble those found in more ordered phases with $R\bar{3}m$ and $C2/m$ space groups. The latter corresponds to the partial honeycomb Li–Mn ion ordering in the LMR cathode, consistent with the ^{7}Li NMR spectra of this material reported previously, which contained a resonance at close to 1500 ppm assigned to Li surrounded by 6 Mn^{4+} ions in the transition metal (TM) layers.[13] Our LMR cathodes were then paired with commercial $Li_4Ti_5O_{12}$ (LTO) anodes and are cycled with two types of electrolytes: a commercial LP57 electrolyte (1 M $LiPF_6$ in EC/ EMC, 3 : 7 in volume ratio) and a pure EMC electrolyte (1 M $LiPF_6$ in EMC). LTO is used as an anode in this study because it does not require EC to produce a stable SEI (solid electrolyte interface) as is the case with graphite, and it simplifies the interpretation of the degradation processes.[14]

Figure 1c shows the first cycle charge–discharge curve for an LMR||LTO full cell in a voltage range of 0.5–3.2 V. During the first charging process, all cells first show a typical sloping region corresponding to Ni^{2+} oxidation to Ni^{4+} and a plateau assigned to the anionic (O^{2-}) oxidation process.[15] The plateau region is shorter for cells with the pure EMC electrolyte resulting in a lower irreversible capacity and a higher first-cycle Coulombic efficiency (82.5% in LP57 and 90.1% in pure EMC electrolyte). Figure S3 (Supporting Information) shows the cycling performance of LMR||LTO full cell with the two different electrolytes at 0.2 C, the full cells with the EMC electrolyte having nearly 91% capacity retention after 100 cycles compared to 81% for LP57. Cells with LP57 electrolyte show a substantial discharge voltage decay (Figure 1d), which was previously shown to arise as a consequence of LMR surface reduction.[13b] The cells with the EMC electrolyte retain a higher discharge voltage as shown in Figure 1e. The average discharge voltage shown in Figure S4 (Supporting Information) for cells with LP57 decreased from 2.04 to 1.71 V (vs LTO–and thus 3.59 and 3.26 vs Li) after 100 cycles (corresponding to a voltage decay rate of 3.23 mV cycle^{-1}) while in cells with the EMC electrolyte, it decreased from 2.05 to 1.86 V (corresponding to the voltage decay rate of 1.88 mV cycle^{-1}). To assess the effectiveness of our approach in suppressing voltage decay with the traditional experimental section, we compared our work with previous studies that employed doping, surface coating, and surface modification, which are summarized in Table S1 (Supporting Information). This table puts our result in the Top 3 of the most effective methods reported to reduce voltage decay in LMR cathodes to our knowledge, in addition, our electrolyte-based approach can be combined with doping and coating strategies to further improve LMR cathode stability. We also verified that the LTO anodes are stable using half cells, which show very good capacity retention of 96.2% after 200 cycles at 0.2 C and 96.6% for 500 cycles at 1 C in LP57 electrolyte (Figure S5, Supporting Information). To decouple the contribution of degradation originating from the LTO anode and LMR cathode, electrochemical tests are further conducted for LTO||Li half-cell with LP57 and pure EMC electrolyte and the results are shown in Figure S6 (Supporting Information). From Figure S6 (Supporting Information), the LTO||Li half cells exhibit very similar charge and discharge capacity and capacity retention rates in both LP57 and pure EMC electrolytes. Therefore, it can be inferred that these two electrolytes do not directly impact LTO anode stability in half cells, however in full cells, cross-talk between the two electrodes might affect anode degradation. Next, we tested LMR||LTO cells for 400 cycles at a rate of 1 C, with 3 slow recovery cycles at 0.2 C performed after every 100 cycles (Figure 1f). The absolute value of the slope for the full cell capacity decay versus cycle number with the two electrolytes at a low rate of 0.2 C and a high rate of 1 C is shown in Figure 1g. The cells with the EMC electrolyte exhibit less capacity decay at both low rate and high rate compared to LP57 electrolyte Further, the capacity loss is more pronounced at 1 C than 0.2 C, which suggests that increases in impedance, possibly due to oxygen loss from the LMR surface, are suppressed by using EC free electrolytes.

An alternative method to investigate the difference in surface reactivity of LMR with different electrolyte components is to measure differences in leakage current after the cell equilibrates on a long voltage hold (VH, here 60 h) at high voltage (here 2.8, 3.0, and 3.2 V vs LTO with a charging rate of 0.05 C). **Figure 2a,b** shows the potential profiles for LMR||LTO cells; note that LTO anodes are very stable with no SEI formation, and therefore, any current measured on the high voltage hold after the cell equilibrates (≈20 h) is probably dominated by reactions taking place at the cathode–electrolyte interface (see Figure 2c,d). The average leakage current increases with the voltage hold potential (Figure 2e), as expected. More importantly, the average oxidation currents for cells without EC solvent are lower at all holding potentials tested here, which indicates that fewer parasitic side reactions are taking place at the cathode-electrolyte interface, in agreement with the cycling results discussed above. Next, the amount of transition metal dissolution and deposition on the anode has been studied by elemental analysis using microplasma atomic emission spectroscopy (MP-AES). These experiments were carried out by cycling LMR||LTO cells for 100 cycles at 0.2 C, after this, the cycled electrolytes and the LTO anodes were retrieved and digested to

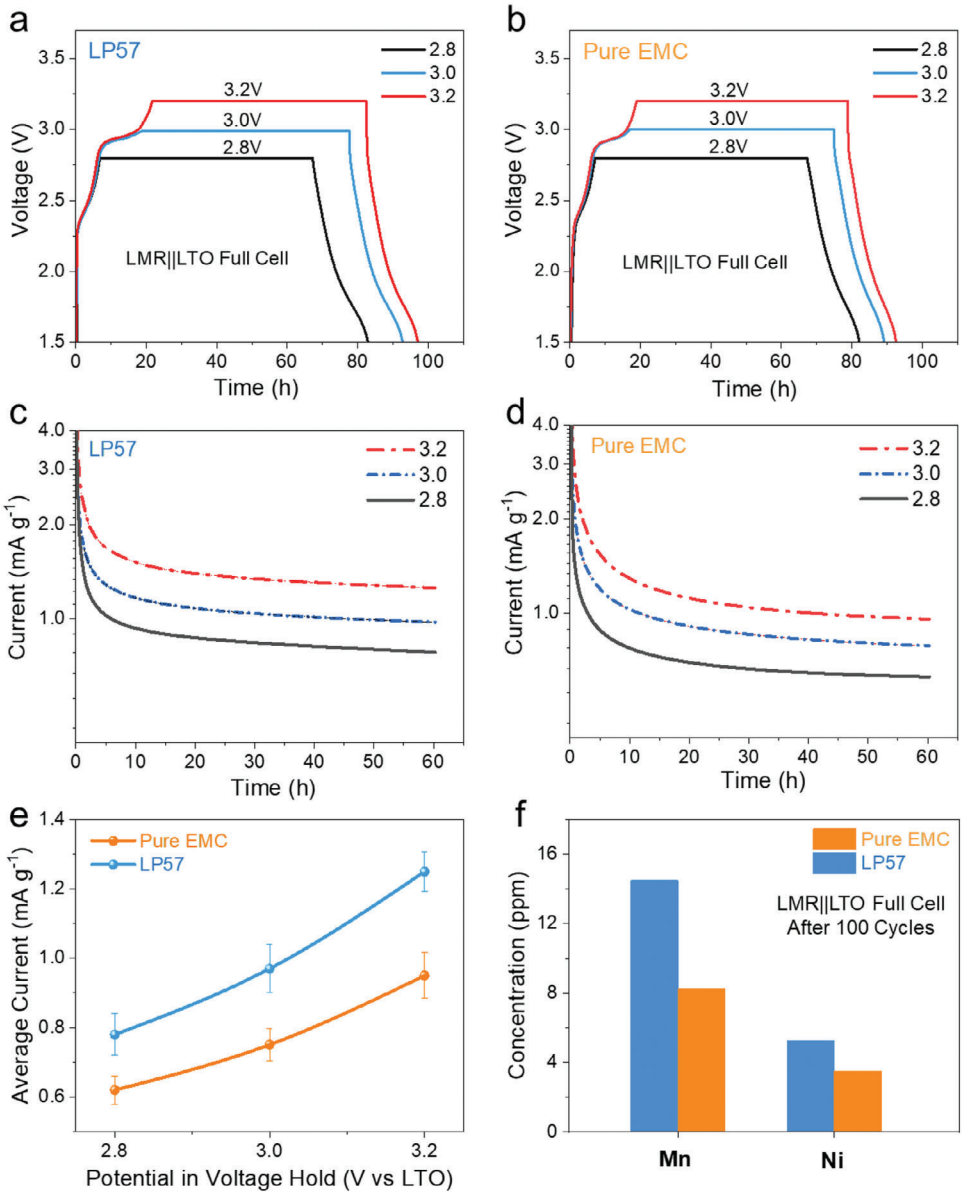

Figure 2. a) Representative potential profiles for LMR||LTO full cells with (a) a LP57 electrolyte and b) an EMC electrolyte during a 0.05 C charge to 2.8, 3.0, and 3.2 V, 60 h voltage hold (VH) and 0.05 C discharge. Oxidation currents, which were normalized to LMR cathode weight, during voltage holding of 2.8, 3.0, and 3.2 V for the LMR||LTO full cells with c) LP57 electrolyte and d) Pure EMC electrolyte. e) Average current at the end of the VH process as a function of holding potential with LP57 and EMC electrolytes. f) Concentration of transition metal elements Mn and Ni dissolved in the electrolytes after 100 cycles for LMR||LTO full cells.

quantify TM deposition, and the results are shown in Figure 2f and Figure S7 (Supporting Information). Both Mn and Ni are detected in all cycled electrolytes and LTO anodes, with both the amount of Mn and Ni being higher in the case of LP57 compared to the EMC electrolyte.

Next, we directly measure the gas evolution from our LMR||LTO cells using LP57 and pure EMC electrolytes using OEMS. The CO_2 and other gas evolution during the charge, voltage hold, and discharge process are depicted in **Figure 3** and S8 (Supporting Information), revealing more gassing in cells using LP57 (26.2 μmol g^{-1}) compared to cells with pure EMC (20.8 μmol g^{-1}) electrolyte solvent. Building upon our previous research results,[10] it is established that the generation of CO_2 primarily stems from the oxidation of electrolyte solvents with cathode lattice oxygen. Therefore, the diminished CO_2 release during the charge and discharge process further indicates a reduced oxygen release for the LMR cathodes when using pure EMC electrolyte.

To further study the differences in diffusion and impedance build-up in cells with and without EC solvent, galvanostatic intermittent titration (GITT) experiments are conducted after 100 cycles at 0.2 C. As shown in **Figure** 4a, the charge/discharge current

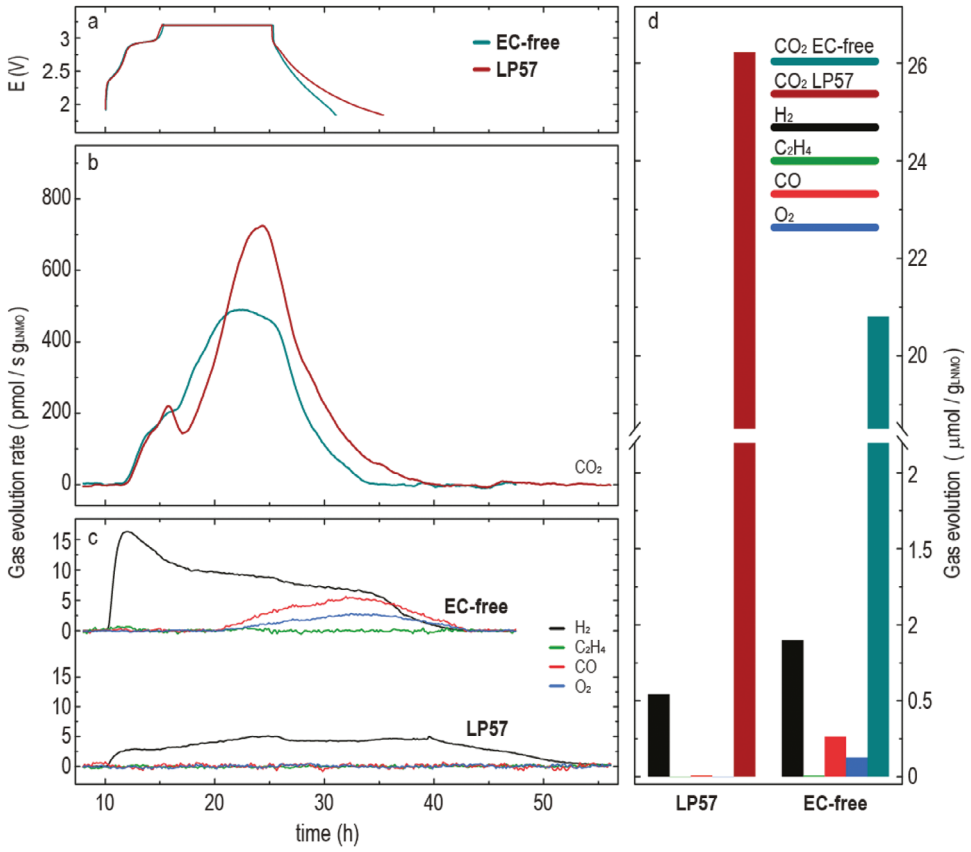

Figure 3. a) Potential profiles for the LMR||LTO full cells during a 0.15 C charge to 3.2 V, 10 h VH, and 0.15 C discharge with LP57 and EMC electrolytes; b) mass spectrometry data corresponding to the evolution of CO_2 (m/z = 44), c) as well as H_2, C_2H_4, CO and O_2 (m/z = 2, 27, 28 and 32, respectively), normalized to the mass of the LMR; d) Total gas generation from each channels quantified in the mass spectrometry data.

pulses are applied at a rate of 0.1 C for 2 h, followed by a 12 h relaxation. From the GITT experiments, the ohmic polarization, equilibrium voltage, and voltage polarization for LMR||LTO cells with LP57 and EMC electrolytes are calculated as a function of SOC, as shown in Figure 4b,c,e,f and Figure S9 (Supporting Information), respectively. The ohmic polarization corresponds to the voltage difference before and immediately after the current pulse is applied (Figure S9a,b, Supporting Information).[16] It is clear from the above results that in both charge and discharge processes, the cell cycle with the EMC electrolytes shows less ohmic polarization, which is in agreement with the above observations made at different cycling rates (shown in Figure 1f). The equilibrium potentials after relaxation for 12 h are almost identical for the cells with or without EC solvent. This further indicates that the bulk of the material remains the same in both cases and shows that degradation is dominated by the cathode surface. To further understand the difference in the Li-ion diffusion in cells with and without EC solvent, the apparent Li-ion diffusion coefficients during the charge and discharge process are calculated from the GITT results. During the charging and discharging process after 100 cycles, the Li-ion diffusion rate is significantly reduced in the cell with LP57 electrolyte at every SOC compared to the cell with the EMC electrolyte (Figure 4f,g), which is also consistent with the result that the overpotential has increased in the cell with LP57 electrolyte (Figure S9c,d, Supporting Information). Previous work on LMR cathodes has shown that the surface-reduced layer, which results from side reactions with the electrolyte, increases the electrode impedance.[13b] As cycling, progresses, we observe a continuous increase in impedance, which might be linked to the surface-reduced layer growing in the sub-surface of the cathode and degrading Li-ion transport. Differences in the impendence build-up in different electrolyte systems are monitored by electrochemical impedance spectroscopy (EIS) over cycling, which is shown in Figure S10 (Supporting Information). In order to compare the impedance of different cells, the EIS data was fitted with an equivalent circuit model (insert figure in Figure S10, Supporting Information) with the ZsimpWin software, and the fitting parameters are shown in Table S2 (Supporting Information). R_s is the high-frequency series resistance, R_{ct} corresponds to the charge transfer resistance, CPE is the cell capacitance, and W_1 is the diffusion Warburg component. The charge-transfer resistances (R_{ct}) in the cell with EMC electrolyte after the 50th and 100th cycles are 322.1 and 535.3 Ω, respectively, whereas for cells with LP57 electrolyte, they are 419.2 and 727.9 Ω, respectively. Table S3 and Figure S11 (Supporting Information) show EIS fitting results of R_W (Warburg resistance, namely the real part of the Warburg element W) and the R_{ct} (charge-transfer resistance) after different numbers of cycles and using different electrolytes in LMR||LTO full cells. This table indicates that during cycling, both R_{ct} and R_W increase, and R_{ct} increases faster than R_W, which may suggest the surface degradation of the LMR cathode material predominates over bulk degradation. All the above

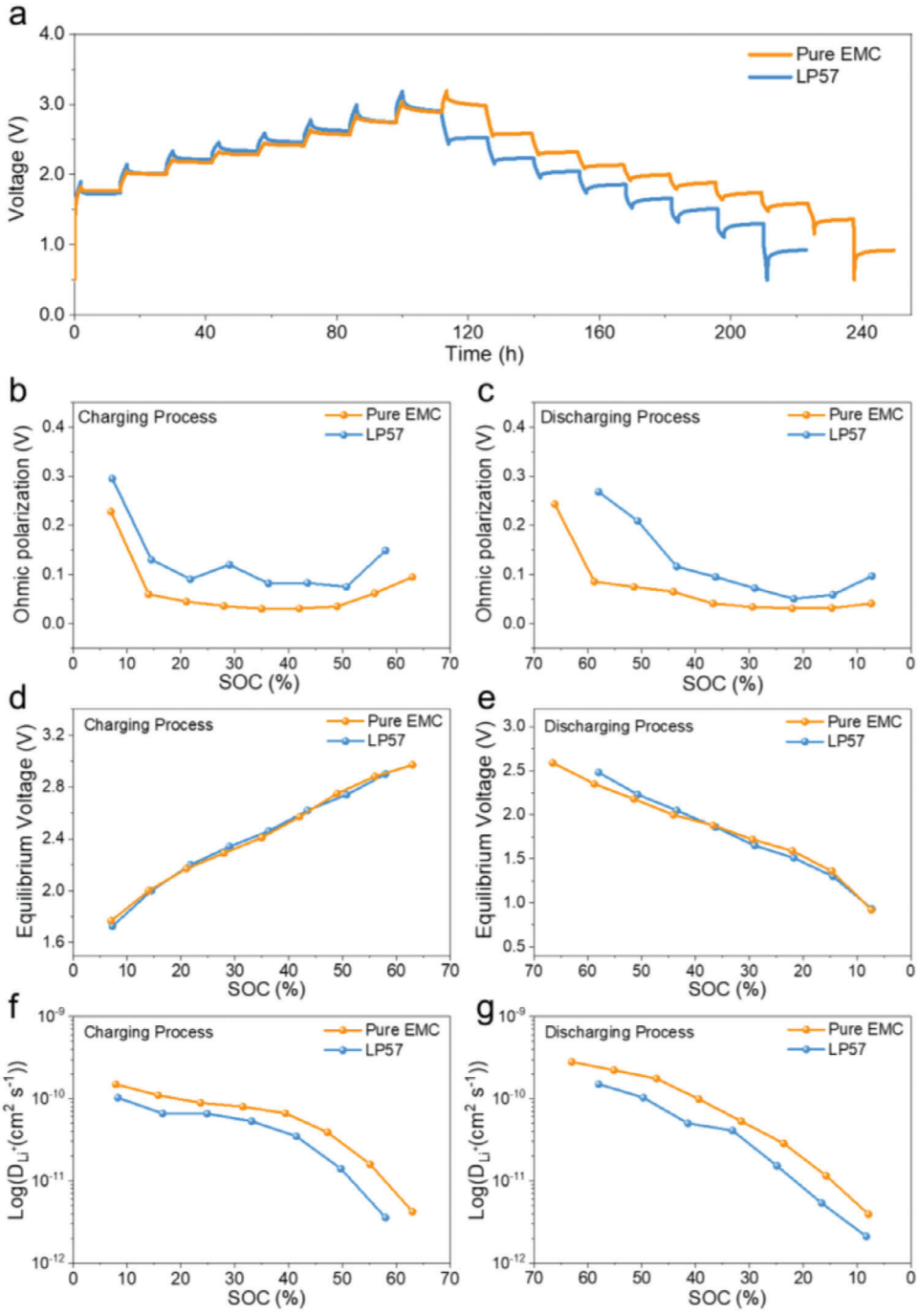

Figure 4. Electrochemical GITT measurements. a) GITT curves of LMR||LTO full cells with LP57 and EMC electrolytes for the 100th electrochemical cycle at 0.2 C during the voltage range from 0.5 to 3.2 V. The corresponding ohmic polarization during the b) charging and c) discharging processes of the LMR||LTO full cells with LP57 and EMC electrolytes for the 100th cycle. Equilibrium voltages during the d) charging and e) discharging processes of the LMR||LTO full cells with LP57 and EMC electrolytes for the 100th cycle. The lithium-ion diffusion coefficients extracted from the GITT measurements are plotted on a log scale during the f) charging process and g) discharging process of the LMR||LTO full cells for the 100th cycle.

results support the hypothesis that more oxygen is lost from the LMR surface in cells using LP57 electrolyte to form a rock-salt or spinel-like layer, with poor Li transport through it,[5b,13b,17] which in turn results in substantial impedance build up in the cells.

It has been proposed that the voltage decay in LMR cathode materials is related to the impedance build-up discussed above,[13b] as well as the lower redox potential of the Mn^{3+}/Mn^{4+} couple, because a proportion of Mn^{4+} will be reduced to compensate for the lattice oxygen loss.[18] Therefore, we studied the

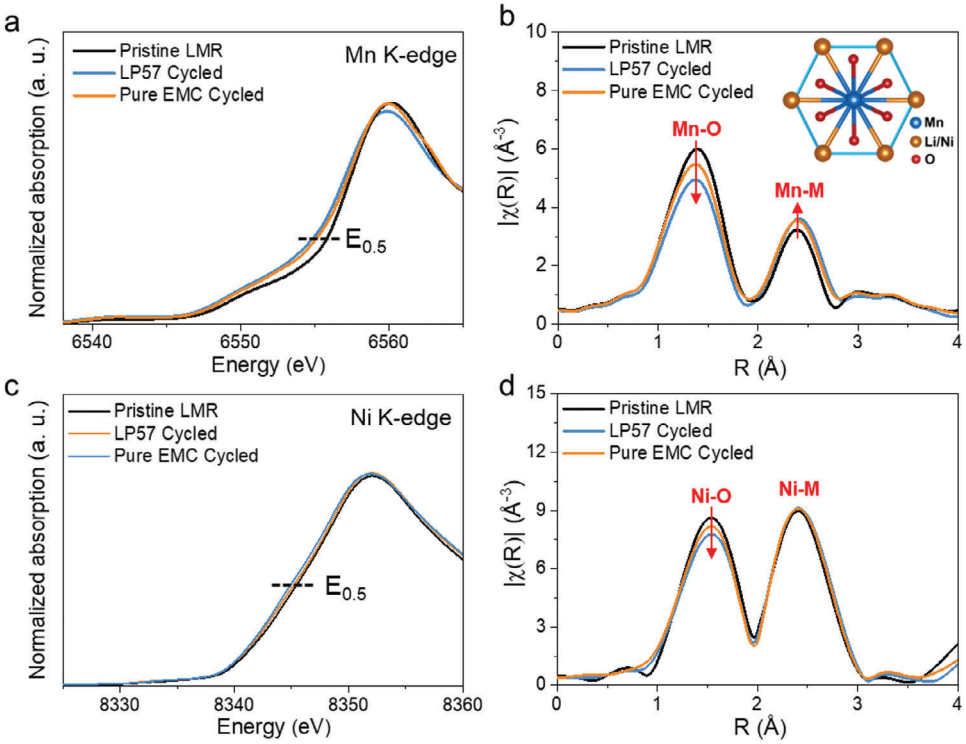

Figure 5. Normalized XANES spectra of the a) Mn K-edge and b) corresponding k^3-weighted Fourier transforms for the Mn absorption of the pristine LMR and cycled LMR cathodes with LP57 electrolyte and EMC electrolytes. Normalized XANES spectra of the c) Ni K-edge and d) corresponding k^3-weighted Fourier transforms for the Ni absorption of pristine LMR and cycled LMR cathodes with LP57 electrolyte and EMC electrolyte.

valence state and electronic structures of Mn, Ni, and O by XAS and (X-ray Photoelectron Spectroscopy) XPS. The normalized X-ray absorption near edge structure (XANES) spectra of Mn K-edge for the pristine LMR cathode and after cycling it 100 times for LP57 and EMC electrolytes are shown in **Figure** 5a. Compared to the LMR cathode cycled with the EMC electrolyte, the Mn K-edge of the LMR cathode cycled with LP57 is shifted slightly toward lower energy, indicating that the LMR cathode cycled with the LP57 electrolyte has a lower average Mn valence state; this in agreement with the voltage decay for the LMR cathodes. To further study the local structure change after 100 cycles with different electrolytes, the corresponding k^3-weighted Fourier transforms for the Mn K-edge extended X-ray absorption fine structure (EXAFS) are also calculated and shown in Figure 5b. The inset schematic in Figure 5b shows the coordination environment for the Mn-ions. The first peak at ≈1.5 Å in the Fourier-transformed EXAFS spectra corresponds to the Mn–O interaction and the second peak at ≈2.5 Å in the Fourier-transformed EXAFS spectra corresponds to the Mn-TM interaction.[13b,19] Comparing the pristine and cycled LMR cathode, the intensity for the first peak of the pristine LMR cathode is higher than that of the cycled LMR cathode, while the intensity for the second peak of pristine LMR cathode is lower than that from the cycled LMR cathode. This is ascribed to the gradual densification of the layered structure due to both oxygen loss and loss of Li from the transition metal that occurs during cycling.[20] Further, the intensity of the first peak at ≈1.5 Å for the LMR cathode cycled with LP57 is lower than that of the cathode cycled in the EMC electrolyte, which also confirms that there is more oxygen loss in the former. Figure 5c shows no significant difference in the Ni K-edge energy position after 100 cycles, indicating very little difference in the Ni oxidation states for the pristine LMR and cycled LMR cathode. The corresponding Fourier transforms for the Ni K-edge extended EXAFS in Figure 5d show two peaks. The first peak at ≈1.5 Å corresponds to the Ni—O bonds and the second peak at ≈2.5 Å corresponds to the Ni-TM interaction.[13b,19] There is little difference in the Ni-TM interaction for the pristine LMR cathode and cycled LMR cathode: only the peak intensities for the Ni—O bonds for the cycled LMR cathodes have decreased slightly due to the oxygen loss during the cycling process.

High-resolution synchrotron XRD was then conducted to study the differences in the crystal structures for the LMR cathodes cycled in the two electrolytes (Figure S12, Supporting Information). Both LMR cathodes exhibit an ideal layered structure (R-3m space group) without any impurity phases, which means that there are no prominent differences in the bulk structure for the LMR cathode cycled with LP57 and EMC electrolytes. There is a slight difference in the $I_{(003)}/I_{(104)}$ value, which suggests that more cation mixing between the Li and TM layers occurs for the LMR cathode particles cycled with LP57 electrolyte; this is ascribed to the more severe oxygen loss that occurs in this system. The GITT results indicate that there is no significant change in equilibrium potential for LMR||LTO full cells with LP57 and pure EMC electrolyte, in agreement with the XAS and XRD results that show that there is little change in the bulk for the cycled LMR cathode with LP57 and pure EMC electrolyte. However, the overpotential and Li-ion diffusion rate for the LMR||LTO full cell cycled with LP57 is obviously worse than that for the full cell cycled with

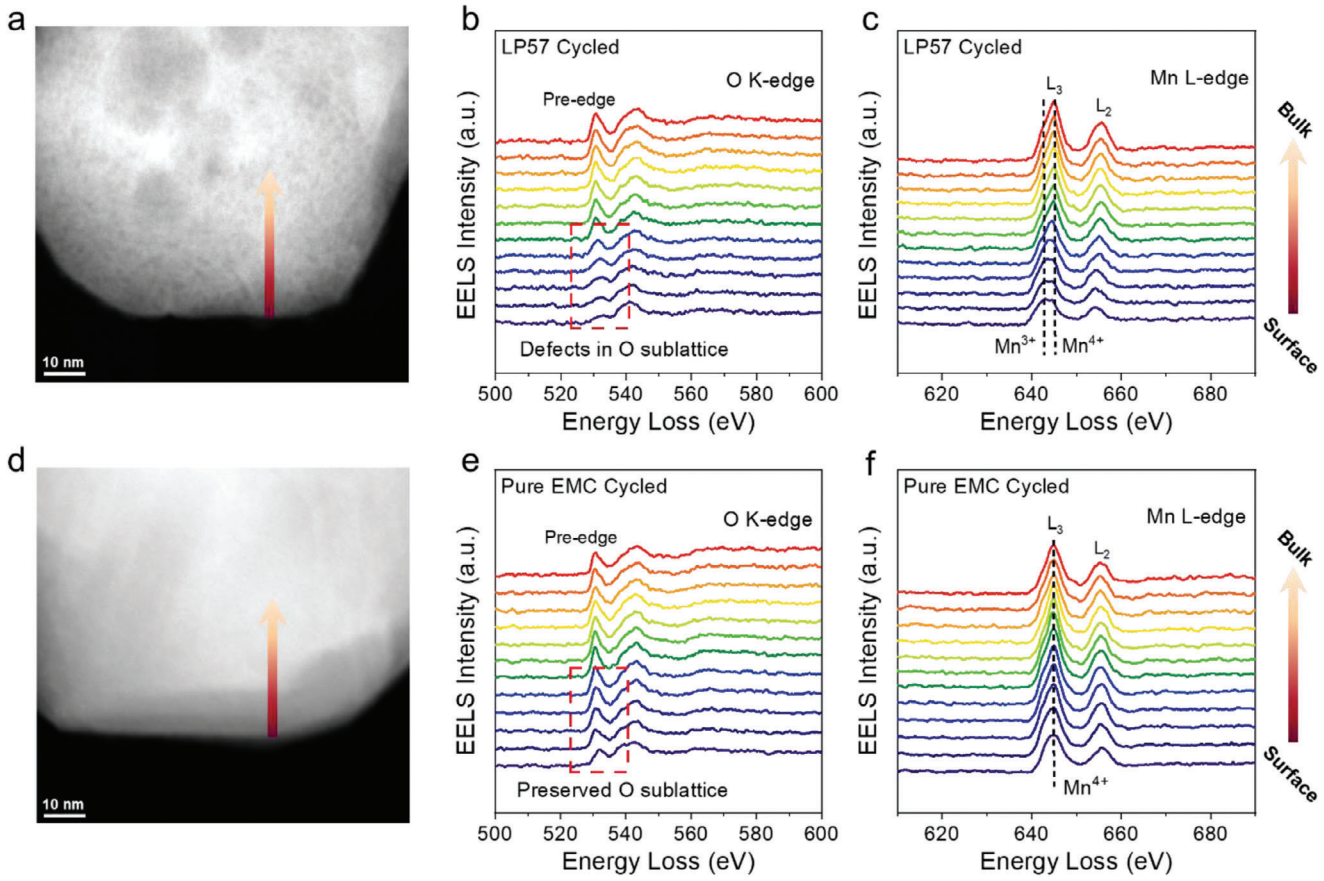

Figure 6. STEM-EELS analysis for LMR cathode. a) STEM-HAADF image and corresponding EELS line scan results of b) O K-edge and c) Mn L_2-edge and L_3-edge of LMR cathode after 100 cycles with LP57 electrolyte. d) STEM-HAADF image and corresponding EELS line scan results of e) O K-edge and f) Mn L_2-edge and L_3-edge of LMR cathode after 100 cycles with pure EMC electrolyte.

EMC. Thus, it can be concluded that the difference in the overpotential and Li-ion diffusion rate is largely caused mainly by surface reduction and oxygen release from the particle surface.[13b]

To further study the differences in elements valence state on the cathode particle surface, XPS tests were carried out as shown in Figures S13 and S14 (Supporting Information). The Mn $2p_{3/2}$ data for the LMR cathodes cycled with different electrolytes show that the proportion of Mn^{3+} when using pure EMC electrolyte is only 15% compared to 54% in the case of LMR with LP57 electrolyte. This means that the surface layers contain more Jahn–Teller distortion caused by Mn^{3+} for cycled LMR cathode with LP57. In addition, as shown in Figure S15 (Supporting Information), the intensity of the pre-edge peak for the cycled LMR cathode with LP57 is higher than the cycled LMR cathode with EMC electrolyte. This also means more distortions in the Mn coordination environments[21] in cycled LMR cathode with LP57, which is consistent with the aforementioned XPS results. The O 1s XPS plots for cycled LMR cathodes with different electrolytes fit well with three peaks as depicted in Figure S13c,d (Supporting Information). These three peaks, at bonding energies of 528.95, 532.40, and 534.57 eV, suggest the presence of lattice oxygen (TM-O), Li_2CO_3/C═O species, and C—O species on the surface of LMR cathode particles, with the latter two products mainly attributed to electrolyte decomposition.[22] The fitting results of the O 1s XPS patterns, shown in Figure S14b (Supporting Information) indicate that the proportion of electrolyte decomposition products on cycled LMR cathodes with EMC electrolyte is much lower than that of cycled LMR cathode with LP57, which further confirms that side reactions on the LMR particle surface are suppressed when cycling with EMC electrolyte. Furthermore, the F 1s XPS analysis (see Figure S16, Supporting Information) shows two peaks, one corresponding to Li—F bond (LiF) at ≈685.3 eV and one to C–F and P–F (C–F/P–F containing species in the CEI and PVDF) bond at ≈687.7 eV.[23] The fitting results for the F 1s XPS suggest that the proportion of LiF in the CEI layer is higher for cells using pure EMC electrolytes. However, more analysis is needed before drawing any further conclusions from this.

To map and investigate oxygen release from the LMR surface and sub-surface, high-angle annular dark field scanning transmission electron microscopy (HAADF-STEM) imaging and EELS analysis are carried out. **Figure 6**a,c,d,f show the HAADF-STEM images and corresponding EELS line scans of O K-edge and Mn L-edge for the LMR cathode cycled with LP57 electrolyte and pure EMC electrolyte, respectively. EELS line scans are plotted from the surface to bulk in steps of 2 nm, and the oxygen pre-edge peak at ≈530 eV can be ascribed to the electron transition from O 1s core state to the unoccupied 2p states.[24]

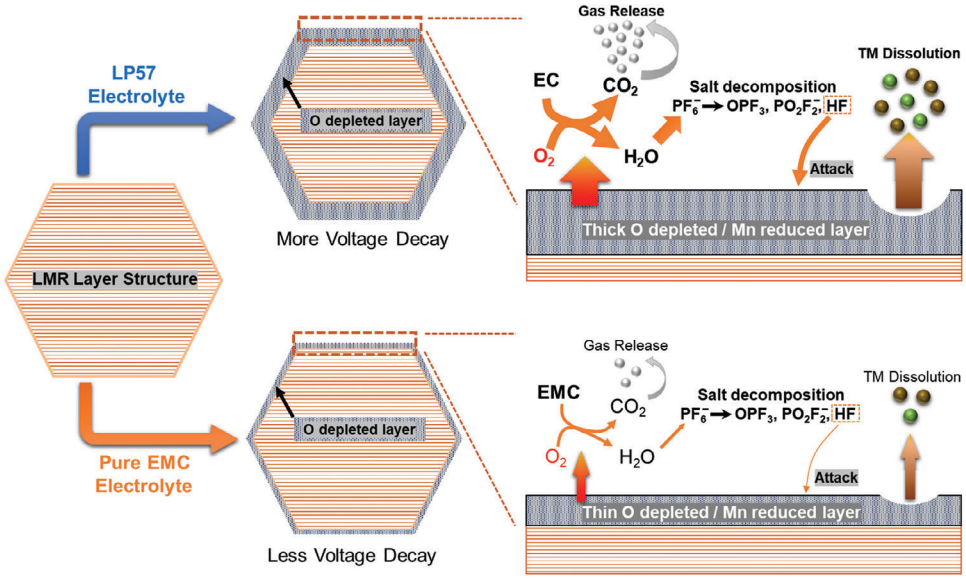

Figure 7. Schematic diagram of particle degradation for the cycled LMR cathode with LP57 and pure EMC electrolyte.

After background subtraction and corrections to account for thickness variations, the relative intensity of the oxygen pre-edge peak for the LMR cathode cycled with LP57 electrolyte exhibits a gradual strengthening from the particle surface to the bulk, implying that there are oxygen defects in the oxygen sublattice, which is again ascribed to reactions between the cathode and electrolyte leading to irreversible oxygen loss. We observed less difference in the relative intensity of oxygen pre-edge peak for LMR cathode cycled with pure EMC electrolyte from particle surface to the bulk, which suggests that oxygen local environments are better preserved within the sublattice. Furthermore, Figure 6c shows that the Mn L_3-edge peak shifts toward lower energy at the particle surface for particles cycled with LP57 electrolyte suggesting that the Mn oxidation state is reduced on the surface.[17] In the case of LMR cycled in pure EMC electrolyte solvent, shown in Figure 6f, the valence state of Mn remains constant at the surface. In addition, Raman spectroscopy, shown in Figure S17 (Supporting Information), indicates that after 100 cycles, a local environment close to that found in a spinel phase ($LiMn_2O_4$, average Mn valence state is +3.5) appears on the LMR surface.[25] Fitting results (see Figure S18, Supporting Information), show that there is less spinel phase in LMR cycled with pure EMC. Overall, both EELS and Raman results indicate that LMR cathodes cycled with pure EMC electrolyte have less oxygen loss from the particle surface.

Overall, the observed increase in lattice oxygen loss when using LMR cathodes is somewhat unexpected because previous studies on NMC have shown that Ni-rich (NMC811) cathodes benefit from EC free electrolytes[16] whereas standard (NMC111) cathodes show no significant difference in oxygen-loss when using EC or EMC electrolyte solvent. Our LMR cathodes have a relatively low Ni content and one might expect them to show little sensitivity to the presence of EC solvent. However, an important difference between low-nickel content NMC and LMR cathodes is that in the latter, O^{2-} is oxidized during the charging process. These oxygen redox reactions might be the reason for the increase in oxygen loss from the cathode surface in the presence of EC, despite the relatively low Ni content of our LMR cathodes. Consistent with this, high Ni-content NMCs, where there is a greater Ni–O covalency and a greater involvement of the oxygen in the redox process also show O-loss.[26] A schematic clarifying the different degradation pathways is shown in **Figure 7**. Reactions between EC and lattice oxygen lead to the formation of CO_2 and H_2O, which in turn leads to further reactions with $LiPF_6$ salt generating HF.[27] The latter is known to etch the cathode surface and lead to further degradation processes linked to TM dissolution.[28] Cells using pure EMC electrolyte solvent show less oxygen loss from the cathode surface, which suppresses the chain of degradation reactions discussed above, resulting in improvements in both capacity and discharge voltage shown in Figure 1.

3. Conclusion

In conclusion, we proposed a novel approach to suppress both voltage decay and capacity fade in LMR cathodes by exploring interactions between different electrolyte solvents and oxygen loss from the cathode surface. In particular, we focused on the effect of EC on the oxygen loss from the cathode surface. SXRD as well as GITT analysis show that the presence of EC solvent does not change the bulk of the material substantially, but XAS, EELS, and Raman analysis shows an increase in oxygen loss from the surface when EC solvents are used in the electrolyte. This increase in surface reactions was measured electrochemically using leakage current analysis as well as OEMS analysis and we found that this goes hand in hand with an increased dissolution of Ni and Mn. Galvanostatic cycling test of LMR versus LTO cells shows that an electrolyte composed of an EMC solvent only shows an increase in capacity retention of 75% after 400 cycles compared to electrolytes that contain both EMC and EC. Overall, our findings suggest that the new electrolyte design is a promising strategy that complements current

research on LMR doping and coatings, to improve LMR cycling stability.

Supporting Information

Supporting Information is available from the Wiley Online Library or from the author.

Acknowledgements

The present research had been supported by the Faraday Institution degradation (FIRG001 and FIRG024) and FutureCAT (FIRG017 and FIRG065) as well as the ERC (Consolidator Grant, MIGHTY, 866005). The authors thank Hwee Jien Tan for assistance with the MP-AES measurements and Wenhai Ji and Mihai Chu for XAS measurements and useful discussions. The author also thanks Debashis Tripathy for assistance with the OEMS experiment and Wesley M. Dose for the development of experimental methods. The authors also acknowledge I11 beamline for synchrotron XRD under the BAG proposal (CY28349). I.T. acknowledges support from a Beatriz Galindo senior fellowship (BG22/00148) from the Spanish Ministry of Science and Innovation.

Conflict of Interest

The authors declare no conflict of interest.

Data Availability Statement

The data that support the findings of this study are available from the corresponding author upon reasonable request.

Keywords

EC-free electrolyte, Li-rich cathode, oxygen loss, voltage decay

Received: March 10, 2024
Revised: May 11, 2024
Published online:

[1] a) J. M. Tarascon, M. Armand, *Nature* **2001**, *414*, 359; b) M. Li, J. Lu, Z. W. Chen, K. Amine, *Adv. Mater.* **2018**, *30*, 1800561.
[2] a) W. He, W. B. Guo, H. L. Wu, L. Lin, Q. Liu, X. Han, Q. S. Xie, P. F. Liu, H. F. Zheng, L. S. Wang, X. Q. Yu, D. L. Peng, *Adv. Mater.* **2021**, *33*, 2005937; b) P. Rozier, J. M. Tarascon, *J. Electrochem. Soc.* **2015**, *162*, A2490; c) H. Zhao, W. Y. A. Lam, L. Sheng, L. Wang, P. Bai, Y. Yang, D. S. Ren, H. Xu, X. M. He, *Adv. Energy Mater.* **2022**, *12*, 2103894.
[3] W. B. Hua, M. Z. Chen, B. Schwarz, M. Knapp, M. Bruns, J. Barthel, X. S. Yang, F. Sigel, R. Azmi, A. Senyshyn, A. Missiul, L. Simonelli, M. Etter, S. N. Wang, X. K. Mu, A. Fiedler, J. R. Binder, X. D. Guo, S. L. Chou, B. H. Zhong, S. Indris, H. Ehrenberg, *Adv. Energy Mater.* **2019**, *9*, 1803094.
[4] a) J. L. Shi, J. N. Zhang, M. He, X. D. Zhang, Y. X. Yin, H. Li, Y. G. Guo, L. Gu, L. J. Wan, *ACS Appl. Mater. Interfaces* **2016**, *8*, 20138; b) X. K. Ju, X. Hou, Z. Q. Liu, L. L. Du, L. Zhang, T. T. Xie, E. Paillard, T. H. Wang, M. Winter, J. Li, *Small* **2023**, *19*, 2207328.
[5] a) S. Cao, J. R. Chen, H. Li, Z. Li, C. M. Guo, G. R. Chen, X. W. Guo, X. Y. Wang, *J. Power Sources* **2023**, *555*, 232398; b) M. Jiang, D. L. Danilov, R. A. Eichel, P. H. L. Notten, *Adv. Energy Mater.* **2021**, *11*, 2103005.
[6] a) Z. W. Yin, S. G. Sun, *Prog. Chem.* **2022**, *34*, 1249; b) K. Zhang, B. A. Li, Y. X. Zuo, J. Song, H. F. Shang, F. H. Ning, D. G. Xia, *Electrochem. Energy Rev.* **2019**, *2*, 606.
[7] D. R. Chen, W. Q. Tu, M. Chen, P. B. Hong, X. X. Zhong, Y. M. Zhu, Q. P. Yu, W. S. Li, *Electrochim. Acta* **2016**, *193*, 45.
[8] a) Y. Y. Hu, Z. Z. Qin, B. W. Cong, J. Pei, S. F. Sun, G. Chen, *ChemElectroChem* **2021**, *8*, 2315; b) Y. J. Liu, X. J. Fan, Z. Q. Zhang, H. H. Wu, D. M. Liu, A. C. Dou, M. R. Su, Q. B. Zhang, D. W. Chu, *ACS Sustainable Chem. Eng.* **2019**, *7*, 2225.
[9] a) Y. P. Deng, Z. W. Yin, G. Wu, S. J. Zhang, F. Fu, T. Zhang, J. T. Li, L. Huang, S. G. Sun, *ACS Appl. Mater. Interfaces* **2017**, *9*, 21065; b) X. H. Zhang, R. Z. Yu, Y. Huang, X. Y. Wang, Y. Wang, B. Wu, Z. S. Liu, J. C. Chen, *ACS Sustainable Chem. Eng.* **2018**, *6*, 12969.
[10] a) W. M. Dose, W. Q. Li, I. Temprano, C. A. O'Keefe, B. L. Mehdi, M. F. L. De Volder, C. P. Grey, *ACS Energy Lett.* **2022**, *7*, 3524; b) W. M. Dose, I. Temprano, J. P. Allen, E. Björklund, C. A. O'Keefe, W. Q. Li, B. L. Mehdi, R. S. Weatherup, M. F. L. De Volder, C. P. Grey, *ACS Appl. Mater. Interfaces* **2022**, *14*, 13206.
[11] K. Zhou, Q. Xie, B. H. Li, A. Manthiram, *Energy Storage Mater.* **2021**, *34*, 229.
[12] Y. W. Li, S. Y. Xu, W. G. Zhao, Z. F. Chen, Z. X. Chen, S. N. Li, J. T. Hu, B. Cao, J. Y. Li, S. S. Zheng, Z. W. Chen, T. L. Zhang, M. J. Zhang, F. Pan, *Energy Storage Mater.* **2022**, *45*, 422.
[13] a) C. P. Grey, N. Dupré, *Chem. Rev.* **2004**, *104*, 4493; b) B. Wen, F. N. Sayed, W. M. Dose, J. K. Morzy, Y. Son, S. Nagendran, C. Ducati, C. P. Grey, M. F. L. De Volder, *J. Mater. Chem. A* **2022**, *10*, 21941.
[14] R. C. McNulty, E. Hampson, L. N. Cutler, C. P. Grey, W. M. Dose, L. R. Johnson, *J. Mater. Chem. A* **2023**, *11*, 18302.
[15] S. Q. Zhao, K. Yan, J. Q. Zhang, B. Sun, G. X. Wang, *Angew. Chem. Int. Ed.* **2021**, *60*, 2208.
[16] H. Yang, R. M. Gao, X. D. Zhang, J. Y. Liang, X. H. Meng, Z. Y. Lu, F. F. Cao, H. Ye, *Adv. Mater.* **2022**, *34*, 2204835.
[17] T. C. Liu, J. J. Liu, L. X. Li, L. Yu, J. C. Diao, T. Zhou, S. N. Li, A. Dai, W. G. Zhao, S. Y. Xu, Y. Ren, L. G. Wang, T. P. Wu, R. Qi, Y. G. Xiao, J. X. Zheng, W. Cha, R. Harder, I. Robinson, J. G. Wen, J. Lu, F. Pan, K. Amine, *Nature* **2022**, *606*, 305.
[18] a) M. Gu, I. Belharouak, J. M. Zheng, H. M. Wu, J. Xiao, A. Genc, K. Amine, S. Thevuthasan, D. R. Baer, J. G. Zhang, N. D. Browning, J. Liu, C. M. Wang, *ACS Nano* **2013**, *7*, 760; b) J. M. Zheng, P. H. Xu, M. Gu, J. Xiao, N. D. Browning, P. F. Yan, C. M. Wang, J. G. Zhang, *Chem. Mater.* **2015**, *27*, 1381.
[19] A. Ito, Y. Sato, T. Sanada, M. Hatano, H. Horie, Y. Ohsawa, *J. Power Sources* **2011**, *196*, 6828.
[20] X. Q. Yu, Y. C. Lyu, L. Gu, H. M. Wu, S. M. Bak, Y. N. Zhou, K. Amine, S. N. Ehrlich, H. Li, K. W. Nam, X. Q. Yang, *Adv. Energy Mater.* **2014**, *4*, 1300950.
[21] W. S. Yoon, C. P. Grey, M. Balasubramanian, X. Q. Yang, J. McBreen, *Chem. Mater.* **2003**, *15*, 3161.
[22] a) Q. H. Li, Y. Wang, X. L. Wang, X. R. Sun, J. N. Zhang, X. Q. Yu, H. Li, *ACS Appl. Mater. Interfaces* **2020**, *12*, 2319; b) S. Park, S. Y. Jeong, T. K. Lee, M. W. Park, H. Y. Lim, J. Sung, J. Cho, S. K. Kwak, S. Y. Hong, N. S. Choi, *Nat. Commun.* **2021**, *12*, 838.
[23] a) C. Y. Cui, X. L. Fan, X. Q. Zhou, J. Chen, Q. C. Wang, L. Ma, C. Y. Yang, E. Y. Hu, X. Q. Yang, C. S. Wang, *J. Am. Chem. Soc.* **2020**, *142*, 8918; b) M. Sina, R. Thorpe, S. Rangan, N. Pereira, R. A. Bartynski, G. G. Amatucci, F. Cosandey, *J. Phys. Chem. C* **2015**, *119*, 9762.
[24] M. Yoon, Y. H. Dong, J. Hwang, J. Sung, H. Cha, K. Ahn, Y. M. Huang, S. J. Kang, J. Li, J. Cho, *Nat. Energy* **2021**, *6*, 362.
[25] Z. Xu, X. Z. Guo, J. Z. Wang, Y. F. Yuan, Q. Sun, R. Tian, H. Yang, J. Lu, *Adv. Energy Mater.* **2022**, *12*, 2201323.
[26] A. R. Genreith-Schriever, H. Banerjee, A. S. Menon, E. N. Bassey, L. F. J. Piper, C. P. Grey, A. J. Morris, *Joule* **2023**, *7*, 1623.
[27] a) N. Laszczynski, S. Solchenbach, H. A. Gasteiger, B. L. Lucht, *J. Electrochem. Soc.* **2019**, *166*, A1853; b) W. D. Li, A. Dolocan, J. Y. Li, Q. Xie, A. Manthiram, *Adv. Energy Mater.* **2019**, *9*, 1901152.
[28] R. J. Pan, Z. H. Cui, M. Yi, Q. Xie, A. Manthiram, *Adv. Energy Mater.* **2022**, *12*, 2103806.